

Floquet engineering spin triplet states in unconventional magnets

Pei-Hao Fu,^{1,*} Sayan Mondal,² Jun-Feng Liu,¹ Yukio Tanaka,^{3,4} and Jorge Cayao^{2,†}

¹*School of Physics and Materials Science, Guangzhou University, Guangzhou 510006, China*

²*Department of Physics and Astronomy, Uppsala University, Box 516, S-751 20 Uppsala, Sweden*

³*Department of Applied Physics, Nagoya University, 464-8603 Nagoya, Japan*

⁴*Research Center for Crystalline Materials Engineering, Nagoya University, 464-8603 Nagoya Japan*

(Dated: June 11, 2025)

We consider unconventional magnets with and without spin-singlet s -wave superconductivity and demonstrate the emergence of spin triplet states due to light drives. In particular, we find that a high-frequency linearly polarized light drive induces a spin-triplet density in d -wave altermagnets which does not exist in the static regime and can directly reveal the strength of the altermagnetic field. In this high frequency regime, we also show that linearly polarized light enables the formation of odd-frequency spin-triplet superconducting correlations possessing d -wave and s -wave parities, which can be controlled by the light drive and accessed by measuring the spin density. Moreover, for low-frequency linearly and circularly polarized light drives, we obtain that the types of superconducting correlations is broadened due to presence of Floquet bands, enabling spin-triplet pairs in d - and p -wave unconventional magnets which are absent in the undriven phase.

The control of materials' properties by tailored light is at the forefront of condensed matter physics not only because it deepens our understanding of matter but also due to its potential for emergent phenomena that are absent in the static regime [1–6]. Of special interest is the manipulation of properties by time-periodic light drives, where the Floquet's theorem [7–9] is used to describe the light effects and hence referred to as Floquet engineering [3]. The prospect of Floquet engineering was demonstrated in several systems [2–6], with the most salient example being the prediction of topological phases [1, 10–13] having Floquet bands due to a non-trivial light-matter interaction [14–21]. To a great extent, the intriguing way light interacts with matter is strongly tied to the effect that light has on spin and momentum [10], making systems with relativistic spin-orbit coupling (SOC) [22, 23] promising for novel Floquet phases.

The recent prediction of unconventional magnets (UMs) has opened a new arena where an unusual SOC appears due to nonrelativistic effects [24–27]. UMs possess zero net magnetization, as in antiferromagnets, and a nonrelativistic splitting of energy bands, as in ferromagnets, which then induce anisotropic spin-polarized Fermi surfaces [24, 27]. UMs can be categorized by taking into account the dependence of the unconventional magnetic order with respect to momentum [24], which leads to even- and odd-parity UMs. The simplest UMs that lately attracted an enormous attention have d -wave and p -wave parities, which are commonly referred to as d -wave altermagnets (AMs) [28, 29] and p -wave UMs [30, 31]. The unique spin-momentum properties of UMs have already shown to exotic phases in normal [24–26] and superconducting states [27]. Despite the great promise of the inherent nonrelativistic SOC in UMs, however, the majority of the focus has been devoted to static systems, leaving the effect of time-periodic light drives and hence of Floquet engineering still an open question.

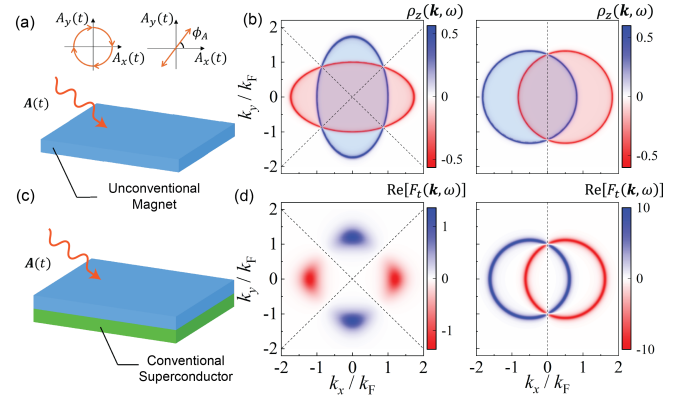


FIG. 1. (a) Sketch of an UM (blue) under a time-periodic light drive $\mathbf{A}(t)$ (orange winkle arrow) with circular or linear polarization. (b) Spin densities along z in the static regime of d -wave AMs and p -wave UMs as a function of k_x and k_y . (c) Sketch of an UM coupled to a conventional spin-singlet s -wave superconductor (green) under a time-periodic light drive $\mathbf{A}(t)$. (d) Real part of the mixed spin-triplet pair amplitude in the static regime of d -wave AMs and p -wave UMs with conventional superconductivity. Parameters: for (b) $M = 0.5$, $\mu = 1$, $k_F = 1$, $\hbar^2/2m = 1$, $\theta_{d,p} = 0$ at frequency $z = 0 + i10^{-3}$; for the d -wave AM and p -wave UM in (d), $\Delta = 0.7\mu$ and $\Delta = 0.25\mu$, respectively, at $z = 0.1\Delta + i10^{-3}$.

In this work, we consider d -wave AMs and p -wave UMs and study their response to a time-periodic light drive in the normal and superconducting states. In general, we demonstrate that the interaction between light and UMs is intrinsically unusual due to the inherent nonrelativistic SOC, giving rise to Floquet-engineered spin-triplet states that are absent in equilibrium. In particular, this unique coupling mechanism enables high-frequency linearly polarized light to induce spin-triplet densities and odd-frequency spin-triplet Cooper pairs with d - and s -wave parities in d -wave AMs. These light-induced spin-

triplet states develop sharp spectroscopic spin-dependent signatures that offer a way to probe the strength and symmetry of the underlying d -wave altermagnetism and emergent pairing. We further show that at low drive frequencies, photon emission and absorption processes couple different Floquet bands, thereby generating Floquet spin-triplet states in both d -wave and p -wave UMs. Our results establish the realization and control of dynamical spin-triplet states in light-driven UMs.

Models for UMs.—We are interested in the effect of light on UMs in the normal and superconducting states, see Fig. 1(a,c). For pedagogical purposes, we first focus on normal state UMs under light, with UMs having d - and p -wave parities. Thus, we model these UMs by [27]

$$H^j(\mathbf{k}) = \xi_{\mathbf{k}} + M_{\mathbf{k}}^j \sigma_z, \quad (1)$$

where $\xi_{\mathbf{k}} = \hbar^2 k^2 / (2m) - \mu$, $\mathbf{k} = (k_x, k_y)$, $k = |\mathbf{k}|$, μ is the chemical potential, $M_{\mathbf{k}}^j$ describes the exchange field of the UM with j -wave parity ($j = d, p$), and σ_z the spin Pauli matrix. Moreover, $M_{\mathbf{k}}^j$ is given by [27]

$$\begin{aligned} M_{\mathbf{k}}^d &= \bar{M}^d [2k_x k_y \sin(2\theta_d) + (k_x^2 - k_y^2) \cos(2\theta_d)], \\ M_{\mathbf{k}}^p &= \bar{M}^p [k_x \cos(\theta_p) + k_y \sin(\theta_p)], \end{aligned} \quad (2)$$

where $\bar{M}^d = M/k_F^2$, $\bar{M}^p = M/k_F$; here, M is the strength of unconventional magnetic order, k_F is the Fermi wavevector, and θ_j is the angle between the x -axis and the lobe of $M_{\mathbf{k}}^j$ [24, 27, 30–34]. From $M_{\mathbf{k}}^d$ at $\theta_d = 0$, the UM is the $d_{x^2-y^2}$ -wave AM, while at $\theta_d = \pi/4$ we have a d_{xy} -wave AM. Similarly, using $M_{\mathbf{k}}^p$ at $\theta_p = 0$ the UM becomes a p_x -wave magnet, while a p_y -wave magnet

is achieved at $\theta_p = \pi/2$. The main property of UMs captured by Eqs. (2) originates from the momentum dependent field $M_{\mathbf{k}}^{d(p)}$, which leads to a momentum dependent spin splitting of bands and spin-polarized anisotropic Fermi surfaces [24, 27]. These properties can be revealed in the spin-density, obtained e. g., by using the retarded Green's function $G^r(\mathbf{k}, \omega) = [\omega + i\eta - H^j(\mathbf{k})]^{-1}$ as $\rho_z(\mathbf{k}, \omega) = (-1/\pi) \text{ImTr}[G^r(\mathbf{k}, \omega) \sigma_z]$ [35, 36]. Hence,

$$\rho_z^j(\mathbf{k}, \omega) = \frac{2}{\pi} \text{Im} \frac{M_{\mathbf{k}}^j}{[M_{\mathbf{k}}^j]^2 - (\omega + i\eta - \xi_{\mathbf{k}})^2}. \quad (3)$$

Thus, the spin density along z is determined by the field $M_{\mathbf{k}}^j$, which can directly probe the d -wave and p -wave parities of UMs, respectively, as we shown in Fig. 1(b).

Non-trivial light-matter coupling and Floquet engineering in UMs.—We now inspect how a light drive affects the main properties of UMs described by Eq. (1). We consider a light drive as a time-periodic field $\mathbf{E}(t)$ with frequency $\Omega = 2\pi/T$ and period T . Then, this time-dependent field is taken into account by a minimal coupling substitution $\mathbf{k} \rightarrow \mathbf{k} + e\mathbf{A}(t)$, where $\mathbf{A}(t)$ is the vector potential due to the light drive $\mathbf{E}(t) = -\partial_t \mathbf{A}(t)$, with $e > 0$ being the fundamental charge. As a result, the time-periodic light drive makes UMs time-dependent. For a generic time-periodic drive $\mathbf{A}(t) = (A_x(t), A_y(t))$, the time-dependent Hamiltonian is given by

$$\hat{H}_{\mathbf{k}}^j(t) = H^j(\mathbf{k}) + V_{\mathbf{k}}^j(t), \quad (4)$$

where $H^j(\mathbf{k})$ is given by Eqs. (1) with a renormalized chemical potential $\mu \rightarrow \mu - e^2 |\mathbf{A}|^2 / (2m)$ and $V_{\mathbf{k}}^j(t)$ reads

$$\begin{aligned} V_{\mathbf{k}}^d(t) &= \frac{\hbar^2}{m} \mathbf{k} \cdot \mathbf{A} + 2\bar{M}^d \{ \bar{\mathbf{k}} \cdot \mathbf{A}(t) \cos(2\theta_d) + [\bar{\mathbf{k}} \times \mathbf{A}(t)]_z \sin(2\theta_d) \} \sigma_z \\ &\quad + \bar{M}^d [A_{x^2-y^2}(t) \cos(2\theta_d) + 2A_{xy}(t) \sin(2\theta_d)] \sigma_z, \\ V_{\mathbf{k}}^p(t) &= \frac{\hbar^2}{m} \mathbf{k} \cdot \mathbf{A} + \bar{M}^p \boldsymbol{\alpha} \cdot \mathbf{A}(t) \sigma_z, \end{aligned} \quad (5)$$

where $\bar{\mathbf{k}} = (k_x, -k_y)$, $A_{x^2-y^2}(t) = A_x^2(t) - A_y^2(t)$, $A_{xy}(t) = A_x(t)A_y(t)$, $\boldsymbol{\alpha} = (\cos\theta_p, \sin\theta_p)$. Thus, Eqs. (5) uncover the effect of the time-periodic drive $\mathbf{A}(t)$ on UMs. The first term in $V_{\mathbf{k}}^d(t)$ and $V_{\mathbf{k}}^p(t)$ is a trivial term arising due to the parabolic band, while the remaining parts are proportional to σ_z and depend on $\mathbf{A}(t)$, reflecting the effect of the *light drive* on UMs. For d -wave AMs, the second term of $V_{\mathbf{k}}^d(t)$ shows that the time-dependent light drive directly affects the altermagnetic field by linearly coupling to momentum akin to common SOC and that depends on the type of d -wave AM, hence causing a nontrivial light-matter interaction. Moreover, the third term of $V_{\mathbf{k}}^d(t)$ manifests that the time-dependent

drive also affects the altermagnetic field in the form of a Zeeman-like effect which is independent of momentum but still distinct for each type of d -wave AM. For p -wave UMs, the second term of $V_{\mathbf{k}}^p(t)$ is a momentum independent Zeeman-like contribution of the light drive, which, however, strongly depends on the type of p -wave UM.

To further assess the effect of the light drive on UMs, and investigate their spin-dependent properties, it is useful to exploit the time-periodicity of the drive $\mathbf{A}(t+T) = \mathbf{A}(t)$ which makes the obtained time-dependent Hamiltonian also time periodic $\hat{H}_{\mathbf{k}}^j(t+T) = \hat{H}_{\mathbf{k}}^j(t)$. We note that here we consider circularly (C) and linearly (L) polarized light drives described, re-

spectively, by $A_C(t) = A_0(\cos\Omega t, \beta\sin\Omega t)$ and $A_L(t) = A_0\cos\Omega t(\cos\phi, \sin\phi)$, where $A_0 = E_0/\Omega$, $\beta = \pm$ describes the left- and right- handed circularly polarized light (CPL), and ϕ captures the real space polarization direction. We then employ the Floquet theorem [7–9] and decompose the time-dependent Hamiltonian $\hat{H}_{\mathbf{k}}^j(t)$ and solutions of the Schrödinger equation in series of the fundamental frequency of the drive Ω [5]. Thus, the time-dependent eigenvalue problem becomes,

$$\sum_{m'} H_{n,m'}^j(\mathbf{k})\Phi_n^{m'}(\mathbf{k}) = \varepsilon_n\Phi_n^m(\mathbf{k}), \quad (6)$$

where $n, m \in \mathbb{Z}$ are Floquet indices, $H_{n,m'}^j = (H_0^j - m'\hbar\Omega)\delta_{n,m'} + \sum_{n'} H_n^j\delta_{n+n',m'}$, with $n' = \pm 1, \pm 2$ and the Hamiltonian harmonics given by $H_n^j(\mathbf{k}) = (1/T) \int dt \hat{H}_{\mathbf{k}}^j(t)\exp(in\Omega t)$. These Harmonics depend on the applied drive and also on the type of UM, and read

$$\begin{aligned} H_0^j(\mathbf{k}) &= H^j(\mathbf{k}) + \frac{(eA_0)^2 \bar{M}^d}{2} \cos(2\Theta_d)\sigma_z\delta_{j,d}\delta_{l,L}, \\ H_{\pm 1}^j(\mathbf{k}) &= \frac{e\hbar^2 A_0 k}{2m} \left[e^{i\beta\theta_k}\delta_{l,C} + \cos(\Theta_k)\delta_{l,L} \right] \\ &\quad + eA_0 k \bar{M}^d \left[e^{i\Theta_{dk}}\delta_{l,C} + \cos(\Theta_{kd})\delta_{l,L} \right] \sigma_z\delta_{j,d} \quad (7) \\ &\quad + eA_0 \bar{M}^p \left[e^{i\beta\theta_p}\delta_{l,C} + \cos(\Theta_p)\delta_{l,L} \right] \sigma_z\delta_{j,p} \\ H_{\pm 2}^j(\mathbf{k}) &= \frac{(\hbar e A_0)^2}{8m} \delta_{l,L} + \frac{(eA_0)^2 \bar{M}^d}{4} \left[2e^{2i\beta\theta_d}\delta_{l,C} \right. \\ &\quad \left. + \cos(2\Theta_d)\delta_{l,L} \right] \delta_{j,d}\sigma_z, \end{aligned}$$

where $j = p, d$ indicates the type of UM and $l = C(L)$ labels C (L) polarized light. Also, $\Theta_i = \theta_i - \phi$, with $i = d, p, k$, $\Theta_{kd} = \theta_k - 2\theta_d + \phi$, $\Theta_{dk}^{\beta} = 2\theta_d - \beta\theta_k$, $\theta_k = \arctan(k_y/k_x)$. Here, $H_{-n}^j(\mathbf{k}) = [H_{+n}^j(\mathbf{k})]^\dagger$. We have thus reduced a time-dependent problem into a lattice in frequency space with diagonal elements $H_0^j - m\hbar\Omega$, where the nearest-neighbor (next-nearest-neighbor) Floquet bands are coupled by $H_{\pm 1}^j$ ($H_{\pm 2}^j$) by the emission/absorption of one (two) photons. At this point, a few remarks are important on Eq. (6) and Eq. (7). First, the components with $|n| \geq 3$ vanish. Second, for a d -wave AM, there appears in the diagonal term H_0^d a Zeeman-like field generated by a linearly polarized drive with a dependence on the relative direction between the AM lobe θ_d and the spatial light polarization ϕ . Third, the one- and two-photon couplings between Floquet bands acquire nontrivial contribution due to the interplay between unconventional magnetism and light, see second and third elements (second element) in the expressions for $H_{\pm 1}^j$ ($H_{\pm 2}^j$) in Eqs. (7). Interestingly, this nontrivial effect manifests in one- and two-photon coupling processes occurring in d -wave AMs under either CPL or LPL. In contrast, the nontrivial effect in p -wave UMs only produces one-photon coupling processes. These properties are of course reminiscent of the nontrivial light-matter

coupling revealed by Eq. (5) and further unveil the richness of driven UMs.

To further inspect the effect of the light drive on UMs, we now assess the induced spin-density. While one can certainly focus on the spin-density of the Floquet system $\rho_z^F(\mathbf{k}, \omega) = (-1/\pi)\text{ImTr}G_F(\mathbf{k}, \omega + i\eta)$, where G_F is the Floquet Green's function associated to the Floquet Hamiltonian in Eq. (6), to gain fundamental understanding we analytically address the high frequency regime [10, 15, 37–41]. This situation is described by an effective Hamiltonian $H_{\text{eff}} \approx H_0^j + \sum_n [H_{-n}, H_n]/(n\Omega) + \mathcal{O}(\Omega^{-2})$, where H_0^j and $H_{n(-n)}$ are given by Eqs. (7). For all types of considered UMs under LPL and CPL, we find that $[H_{-n}, H_n] = 0$; this implies that light-induced effects appear from H_0^j in the second term of Eq. (7), which is nonzero only for d -wave AMs under linearly polarized light. Thus, under high-frequency LPL, we obtain an effective spin triplet density in d -wave AMs given by

$$\rho_z^{\text{eff}}(\mathbf{k}, \omega) = \rho_{z,M}^{\text{eff}}(\mathbf{k}, \omega) + \rho_{z,\Omega}^{\text{eff}}(\mathbf{k}, \omega), \quad (8)$$

where $\rho_{z,M}^{\text{eff}}(\mathbf{k}, \omega) = (2/\pi)\text{Im}[M_{\mathbf{k}}^d/D_{\Omega}]$ and $\rho_{z,\Omega}^{\text{eff}}(\mathbf{k}, \omega) = (2/\pi)\text{Im}[M_{\Omega}^d/D_{\Omega}]$; here $M_{\Omega}^d = \bar{M}^d e^2 A_0^2 \cos(2\Theta_d)/2$, $A_0 = E_0/\Omega$, and $D_{\Omega} = (M_{\mathbf{k}}^d + M_{\Omega}^d)^2 - (\omega + i\eta - \xi_{\mathbf{k}})^2$. Thus, Eq. (8) implies that LPL induces a finite spin density ($\rho_{z,\Omega}^{\text{eff}}$) in d -wave AMs, which does not vanish at the momenta where the part originated from the static density ($\rho_{z,M}^{\text{eff}}$) does. To elucidate the effect of the LPL, we inspect the spin density integrated over momenta $\bar{\rho}_z^{\text{eff}}(\omega) = [1/(2\pi)^2] \int d\mathbf{k} \rho_z^{\text{eff}}(\mathbf{k}, \omega) \equiv \bar{\rho}_{z,M}^{\text{eff}}(\omega) + \bar{\rho}_{z,\Omega}^{\text{eff}}$. In the strict static regime ($A_0 = 0$), both components of the integrated spin density $\bar{\rho}_z^{\text{eff}}(\omega)$ vanish regardless of the altermagnetic strength M , an effect that is similar to the magnetization of UMs and depicted in Fig. 2 for a driven $d_{x^2-y^2}$ -wave AM; here, the energy bands are only split at $\mathbf{k} \neq 0$ [Fig. 2(f)]. Surprisingly, in the driven phase, both components $\bar{\rho}_{z,M}^{\text{eff}}$ and $\bar{\rho}_{z,\Omega}^{\text{eff}}$ remain finite, leading to a finite light-induced spin triplet density $\bar{\rho}_z^{\text{eff}}$ in d -wave AMs, see Fig. 2. Depending on the altermagnetic field strength M and frequency ω , $\bar{\rho}_{z,M}^{\text{eff}}$ and $\bar{\rho}_{z,\Omega}^{\text{eff}}$ can produce a dominant contribution. In particular, for $M/\mu < 1$ and $\omega/\mu > -1$, the integrated spin density $\bar{\rho}_z^{\text{eff}}$ is negative and its value entirely comes from $\bar{\rho}_{z,\Omega}^{\text{eff}}$, see Fig. 2(a-c). In this case, the spin bands are split for all \mathbf{k} due to the applied drive and the spin density develops a dip centred at $\omega = -\mu$, see dotted and solid blue curves in Fig. 2(d,e).

At $M/\mu = 1$, one of the spin bands becomes dispersionless, resembling a flat band [Fig. 2(f)], and leads to a large spin density due to high density of states, see gray curve in Fig. 2(e). The spin density at $M/\mu = 1$ acquires large values just above and below $\omega/\mu = -1$, forming a dip-peak structure that becomes more evident when M takes larger values. In fact, for $M/\mu > 1$, the two spin split bands exhibit opposite effective masses [Fig. 2(f).], which then makes $\bar{\rho}_{z,M}^{\text{eff}}$ to acquire positive values that are comparable to those of the negative $\bar{\rho}_{z,\Omega}^{\text{eff}}$. As a result, a finite

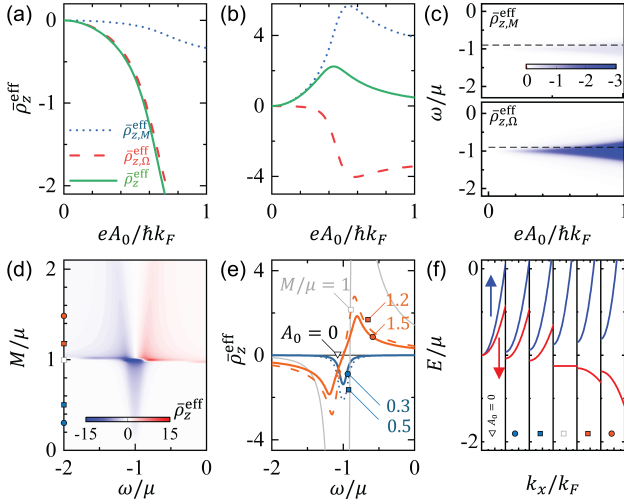


FIG. 2. (a,b) Integrated spin density $\bar{\rho}_z^{\text{eff}}$ (green curve) as a function of A_0 for $M/\mu = 0.5$ (a) and $M/\mu = 1.2$ (b), both at $\omega/\mu = -0.9$ for a $d_{x^2-y^2}$ -wave AM under LPL. The dotted blue and dashed red curves show $\bar{\rho}_{z,M}^{\text{eff}}$ and $\bar{\rho}_{z,\Omega}^{\text{eff}}$, respectively. (c) $\bar{\rho}_{z,M}^{\text{eff}}(\omega)$ and $\bar{\rho}_{z,\Omega}^{\text{eff}}(\omega)$ as a function of ω and A_0 at $M/\mu = 0.5$, where black dashed lines indicate $\omega/\mu = -0.9$. (d) Spin density $\bar{\rho}_z^{\text{eff}}$ as a function of M and ω at $eA_0/(\hbar k_F) = 0.5$, while (e) shows line cuts at distinct values of M marked in (d) and depicted by blue, gray, and orange curves for $M/\mu < 1$, $M/\mu = -1$, and $M/\mu > 1$, respectively. (f) Energy versus k_x at $k_y = 0$ for the distinct values corresponding to the distinct values of M in (e). The spin-up (spin-down) bands are denoted in blue (red). Parameters: $\mu = 1$, $\hbar^2/(2m) = 1$ and $k_F = 1$, $\theta_d = \pi/4$ and $\phi = 0$, $eA_0/(\hbar k_F) = 0.5$.

spin density $\bar{\rho}_z^{\text{eff}}$ appears having a clear dip-peak structure, with a positive value (peak) when $\omega/\mu < -1$ and a negative value (dip) for $\omega/\mu > -1$, see orange curves in Fig. 2(e); this leaves $\bar{\rho}_z^{\text{eff}} = 0$ at $\omega = -\mu$. For $M/\mu > 1$, the dip is centred at $\omega = -\mu - M_\Omega^d$, while the peak is centred at $\omega = -\mu + M_\Omega^d$, where $M_\Omega^d = \bar{M}^d e^2 A_0^2/2$. An important feature of the dip-peak structure seen for $M/\mu > 1$ is that the separation between peak and dip provides a direct way to extract the strength of the altermagnet field: The energy difference $\delta\omega$ between the peak and dip can be measured by microwaves in electron spin resonance spectroscopy [42], where the altermagnet strength is identified as $M = \delta\omega/[(eA_0/\hbar k_F)^2 \cos(2\Theta_d)]$ at $\phi = 0$. At $\phi \neq 0$, $\bar{\rho}_z^{\text{eff}}(\mathbf{k}) \sim \cos(2\theta_d - 2\phi)$, which implies that it is also possible to identify the altermagnet spin splitting and the type of AM, e. g., via optical response. We have also verified that the analysis presented above holds for d_{xy} -wave AMs ($\theta_d = \pi/4$) under linearly polarized light, provided $\phi \neq n\pi/2$ [43].

Floquet engineering spin-triplet Cooper pairs.—Having demonstrated the effect of light drives on UMs, here we assess their impact on UMs with conventional spin-singlet s -wave superconductivity [Fig. 1(c)]. In particular, we address the generation and control of emergent Cooper pairs by means of light drives within the Floquet frame-

work introduced in the previous section. We start by noting that, under a time-periodic drive, UMs with conventional superconductivity are modelled in Nambu space by $\hat{H}_{\text{sc}}^j(\mathbf{k}, t) = H_{\text{sc}}^j(\mathbf{k}) + U_{\mathbf{k}}^j(t)$, where $H_{\text{sc}}^j(\mathbf{k})$ describes the static UM with spin-singlet s -wave superconductivity and $U_{\mathbf{k}}^j$ accounts for the time-dependent drive. The basis of $H_{\text{sc}}^j(\mathbf{k})$ is $\psi_{\mathbf{k}} = (c_{\mathbf{k}\uparrow}, c_{\mathbf{k}\downarrow}, c_{-\mathbf{k}\uparrow}^\dagger, c_{-\mathbf{k}\downarrow}^\dagger)^T$, with T the transpose operation. Here, $H_{\text{sc}}^j(\mathbf{k}) = \xi_{\mathbf{k}}\tau_z + M_{\mathbf{k}}^d\sigma_z\tau_z + M_{\mathbf{k}}^p\sigma_z\tau_0 - \Delta\sigma_y\tau_y$, with τ_i being the i -th Pauli matrix in Nambu space, while $U_{\mathbf{k}}^j(t)$ is a generalized expression in Nambu space of Eq. (5). We are interested in the emergent Cooper pairs in $\hat{H}_{\text{sc}}^j(t)$, which are characterized by the anomalous Green's function [35, 36] $\mathcal{F}_{\sigma_1\sigma_2}(\mathbf{k}_1, \mathbf{k}_2; t_1, t_2) = -i\langle \mathcal{T} c_{\mathbf{k}_1\sigma_1}(t_1) c_{\mathbf{k}_2\sigma_2}(t_2) \rangle$; here \mathcal{T} is the time-ordering operator and $c_{\mathbf{k}\sigma}$ represents the annihilation operator of an electronic state with momentum \mathbf{k} , spin σ , at time t . To demonstrate the emergence of light-induced Cooper pairs, we focus on d -wave AMs under high frequency linearly polarized light. Thus, using the Floquet description of the previous section, we find that the effective Hamiltonian is given by

$$H_{\text{eff}}^d(\mathbf{k}) = H_{\text{sc}}^d(\mathbf{k}) + M_\Omega^d\sigma_z\tau_z, \quad (9)$$

where $H_{\text{sc}}^d(\mathbf{k}) = \xi_{\mathbf{k}}\tau_z + M_{\mathbf{k}}^d\sigma_z\tau_z - \Delta\sigma_y\tau_y$ describes the static Hamiltonian and the second term M_Ω^d appears due to the light drive; see Eqs. (2) and Eq. (8). Then, the emergent Cooper pairs are characterized by the anomalous Green's functions [35, 36] associated to $G_{\text{eff}}^d(\mathbf{k}, \omega) = [\omega + i\eta - H_{\text{eff}}^d(\mathbf{k})]^{-1}$ in Eq. (9), which leads to spin-singlet (s) and mixed spin-triplet (t) pair amplitudes given by

$$F_s^{\text{eff}}(\mathbf{k}, z) = \frac{\Delta\mathcal{P}(z, \Omega, \mathbf{k})}{[\mathcal{P}(z, \Omega, \mathbf{k})]^2 + 4z^2(M_{\mathbf{k}}^d + M_\Omega^d)^2}, \quad (10)$$

$$F_t^{\text{eff}}(\mathbf{k}, z) = \frac{2z\Delta(M_{\mathbf{k}}^d + M_\Omega^d)}{[\mathcal{P}(z, \Omega, \mathbf{k})]^2 + 4z^2(M_{\mathbf{k}}^d + M_\Omega^d)^2},$$

where z represents complex frequencies, $\mathcal{P}(z, \Omega, \mathbf{k}) = [z^2 - (M_{\mathbf{k}}^d + M_\Omega^d)^2 - \xi_{\mathbf{k}}^2 - \Delta^2]$ is an even function of z .

The spin-singlet pairing F_s^{eff} naturally results from the parent conventional superconductor and has an even-frequency spin-singlet even-parity symmetry, which fulfills the antisymmetry condition due to Fermi-Dirac statistics [44–49]. The mixed spin-triplet component F_t^{eff} contains two contributions denoted by $F_{t,M}^{\text{eff}}$ and $F_{t,\Omega}^{\text{eff}}$, respectively: the first term results from the interplay between altermagnetism and the parent superconductor [50], while the second term emerges entirely due to the combined effect of light, altermagnetism and superconductivity. The spin-triplet pairing F_t^{eff} belongs to the odd-frequency mixed spin-triplet even-parity class [27, 50, 51], with its first and second parts having d -wave and s -wave parities, respectively. The driven d -wave AM hence hosts light-induced spin-triplet s -wave superconducting pairs in addition to the d -wave pairs present in the static regime, see Fig. 1(d). This situation is reminiscent of high- T_c superconductors with dominant d -wave

pairing mixed with a s -wave component [52, 53], which can be detected via quasiparticle interference [54–56]. We also find that the spin-triplet pairing is accompanied by a spin-triplet spin density along z given by

$$\rho_{z,sc}^{\text{eff}}(\mathbf{k}, \omega) = \frac{2}{\pi} \text{Im} \left[\frac{\mathcal{Q}(\omega, \Omega, \mathbf{k})}{2\Delta(\omega + i\eta)} F_t^{\text{eff}}(\mathbf{k}, \omega + i\eta) \right], \quad (11)$$

where $\mathcal{Q}(\omega, \Omega, \mathbf{k}) = (\omega + i\eta + \xi_{\mathbf{k}})^2 - (M_{\mathbf{k}}^d + M_{\Omega}^d)^2 + \Delta^2$. In the normal state, when $F_t^{\text{eff}}(\mathbf{k}, z) = 0$, $\rho_{z,sc}^{\text{eff}}$ reduces to the normal state expression given by Eq. (8). In the superconducting state, however, the spin density is tied to the emergent spin-triplet pairing. While this relationship already happens in the static phase, therein the spin density (and hence the spin-triplet pairing) vanishes when integrating over \mathbf{k} , as we discussed before. Hence, a finite spin-triplet pairing appears only due to the light drive.

To visualize the light-induced spin-triplet pairing, in Fig. 3 we plot the integrated pair amplitude $\bar{F}_t^{\text{eff}}(z) = (1/N) \int d\mathbf{k} F_t^{\text{eff}}(\mathbf{k}, z) = \bar{F}_{t,M}^{\text{eff}} + \bar{F}_{t,\Omega}^{\text{eff}}$ as well as its components $\bar{F}_{t,M(\Omega)}^{\text{eff}}$ for a $d_{x^2-y^2}$ -AM. In Fig. 3(a) we show $\text{Re}\bar{F}_t^{\text{eff}}$ as a function of ω and A_0 at $M/\mu = 0.2$ [57], which shows that the drive induces a finite spin-triplet pairing. Fig. 3(a) also shows that $\text{Re}\bar{F}_t^{\text{eff}}$ exhibits a peak-dip structure at the edges of the negative energy bands here denoted by $\omega_{\pm}^{\pm} = \pm M \pm M_{\Omega}^d - \Delta\sqrt{1 - (M/\mu)^2}$ and $\omega_{\Omega}^{\pm} = \pm M_{\Omega}^d - \sqrt{\mu^2 - \Delta^2}$. In the static regime, the energy spectrum of Eq. (9) becomes gapless when $M > M_c \equiv \Delta/\sqrt{1 + (\Delta/\mu)}$, where $\omega_{+}^{\pm} = 0$. In the driven phase, the gap closing is modified by the light induced spin splitting M_{Ω}^d , opening a gap at $k_{x(y)} = 0$ of size $|\omega_{\Omega}^+ - \omega_{\Omega}^-|$. To resolve the peak-dip structure, Fig. 3(b) displays the frequency dependence of $\text{Re}\bar{F}_t^{\text{eff}}$ and of its components $\text{Re}\bar{F}_{t,M(\Omega)}^{\text{eff}}$ at fixed $A_0 \neq 0$. For $\omega \in [\omega_{+}^+, 0]$, both $\text{Re}\bar{F}_{t,M}^{\text{eff}}$ and $\text{Re}\bar{F}_{t,\Omega}^{\text{eff}}$ exhibit equal sign and enhance the total spin-triplet pairing within the superconducting gap corresponding to Fig. 3(c). As ω enters the interval $[\omega_{-}^+, \omega_{+}^+]$, $\bar{F}_{t,M}^{\text{eff}}$ changes sign, inducing a sharp peak-dip structure at $\omega = \omega_{+}^{\pm}$. For $\omega \in [\omega_{-}^+, \omega_{+}^+]$, both components develop opposite signs, suppressing $\text{Re}\bar{F}_t^{\text{eff}}$, see Fig. 3(b,c). At $\omega = \Delta$, $\text{Re}\bar{F}_{t,M}^{\text{eff}}$ and $\text{Re}\bar{F}_{t,\Omega}^{\text{eff}}$ develop opposite signs, giving rise to a vanishing spin triplet pairing. A constructive interference resumes for $\omega \in [\omega_{-}^-, \omega_{+}^-]$ before the spin-triplet pairing is suppressed again for $\omega < \omega_{-}^-$. Interestingly, another sharp peak-dip structure appears at $\omega = \omega_{\Omega}^{\pm}$, where $\text{Re}\bar{F}_t^{\text{eff}}$ is dominated by the light-induced term $\text{Re}\bar{F}_{t,\Omega}^{\text{eff}}$, also seen in Fig. 3(c). Further insights are obtained from Fig. 3(d) which shows $\text{Re}\bar{F}_t^{\text{eff}}$ as a function of ω and the altermagnetic strength M . Here we can see that a large spin-triplet pairing occurs when $M < \mu$ for a broad range of ω . For $M > \mu$, however, a finite spin-triplet emerges for $\omega \in [\omega_{\Omega}^-, \omega_{\Omega}^+]$ with a roughly constant (plateau) value [Fig. 3(e)].

The peak-dip structure for $M/\mu < 1$ and the plateau for $M/\mu > 1$ in the spin-triplet pair amplitude \bar{F}_t^{eff} can be detected via Andreev conductance G_A [58–62]:

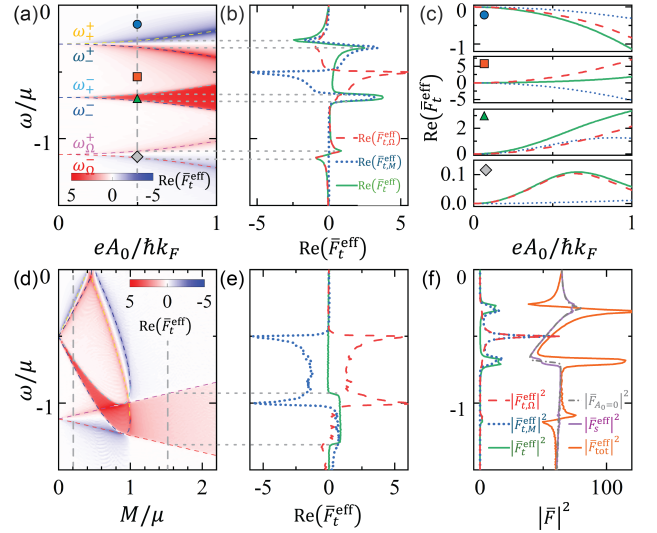


FIG. 3. (a) Real part of the integrated spin-triplet pair amplitude $\text{Re}\bar{F}_t^{\text{eff}}$ as a function of ω and A_0 at $M/\mu = 0.2$ for a $d_{x^2-y^2}$ -wave AM with superconductivity under LPL. Here, ω_{\pm}^{\pm} and ω_{Ω}^{\pm} depicted by dashed curves are the negative band edges of the spectrum of Eq. (9). (b) Line cut of (a) as a function of ω at $eA_0/(\hbar k_F) = 0.5$, where dashed (dotted) curve shows $\bar{F}_{t,M(\Omega)}^{\text{eff}}$. (c) Real part of \bar{F}_t^{eff} , $\bar{F}_{t,M}^{\text{eff}}$ and $\bar{F}_{t,\Omega}^{\text{eff}}$ of (b) as a function of A_0 at ω indicated by markers in (a). (d) $\text{Re}\bar{F}_t^{\text{eff}}$ as a function of ω and M at $eA_0/(\hbar k_F) = 0.5$. (e) Line cut of (d) at $M/\mu = 1.5$. (f) $|\bar{F}_t^{\text{eff}}|^2$ and its singlet and triplet contributions as a function of ω at $M/\mu = 0.2$ and $eA_0/(\hbar k_F) = 0.5$. The gray curve shows $|\bar{F}_t^{\text{eff}}|^2$ at $A_0 = 0$. Parameters: $\Delta = 0.5$ and the rest the same as in Fig. 2.

$G_A \propto |\bar{F}_{\text{tot}}^{\text{eff}}(\omega)|^2 = |\bar{F}_s^{\text{eff}}(\omega) + \bar{F}_t^{\text{eff}}(\omega)|^2$ and it is shown in Fig. 3(f). While $|\bar{F}_{\text{tot}}^{\text{eff}}(\omega)|^2$ is dominated by the spin-singlet term, it exhibits two clear peak-dip features due to the spin-triplet part. The first peak-dip signal occurs at $\omega \sim \omega_{+}^{\pm}$ and is mainly due to $|\bar{F}_{t,M}^{\text{eff}}|^2$, while the second peak-dip feature at $\omega \sim \omega_{\Omega}^{\pm}$ is dominated by $|\bar{F}_{t,\Omega}^{\text{eff}}|^2$. By measuring the peak-dip energy difference, $\delta\omega = |\omega_{+}^+ - \omega_{+}^-| = |\omega_{\Omega}^+ - \omega_{\Omega}^-|$, the altermagnetic strength is extracted as $M = \delta\omega/[(eA_0/k_F)^2 \cos(2\Theta_d)]$, in line with the value obtained from normal state spin density.

While spin-triplet odd-frequency Cooper pairs appear only in d -wave UMs under high-frequency LPL, at low Ω , both odd- and even-frequency spin-triplet pairs emerge in all driven UMs. These superconducting pairs originate from Floquet bands, where the Floquet anomalous Green's functions $F_{n,m}$ obey the anti-symmetry condition $F_{n,m}^{\sigma_1\sigma_2}(\mathbf{k}_1, \mathbf{k}_2, z) = -F_{-m,-n}^{\sigma_2\sigma_1}(\mathbf{k}_2, \mathbf{k}_1, -z)$ [63, 64], with $n, m \in \mathbb{Z}$ and $F_{n,m}$ being the Floquet harmonics of the two-time anomalous Green's function $\mathcal{F}_{\sigma_1\sigma_2}(\mathbf{k}_1, \mathbf{k}_2; t_1, t_2)$ discussed above Eq. (9). This anti-symmetry condition enables pairing between electrons in different Floquet bands via the absorption/emission of $|n-m|$ photons [63]. While multiple pair symmetries are possible, Fig. 4(a) shows the magnitude of the emergent

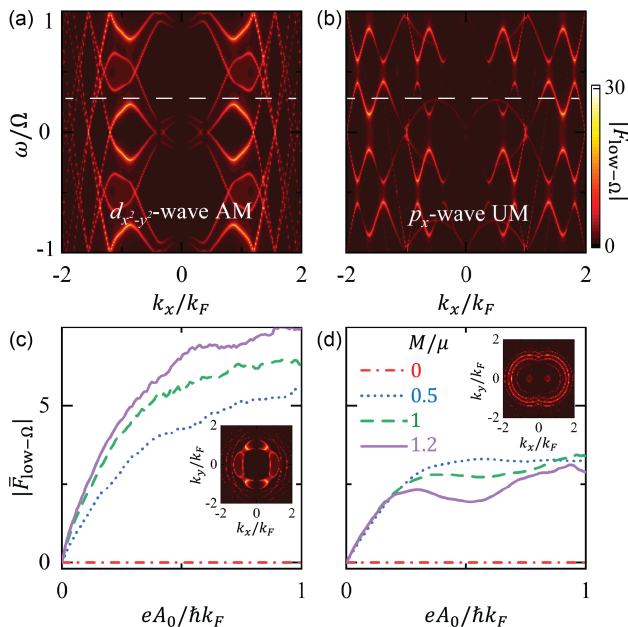


FIG. 4. (a) Absolute value of an emergent spin-triplet odd-Floquet odd-frequency odd-parity pair amplitude $F_{\text{low}-\Omega}$ as a function of ω and k_x at $k_y = 0$ and $M/\mu = 0.5$ in a $d_{x^2-y^2}$ -wave AM ($\theta_d = 0$) with s -wave superconductivity under LPL. (b) Same as in (a) but for an emergent spin-triplet odd-Floquet even-frequency even-parity pair amplitude in a p -wave UM ($\theta_p = 0$). (c,d) Integrated pair amplitudes of (a,b) $\bar{F}_{\text{low}-\Omega}$ as a function of A_0 for distinct M . The inset exhibited the momentum dependence of $\bar{F}_{\text{low}-\Omega}$. Parameters: $\phi = 0$, $\Delta = 0.5$, while the rest same as in Fig. 3.

pairing with spin-triplet odd-Floquet odd-frequency odd-parity as a function of k_x and ω in a $d_{x^2-y^2}$ -wave UM under LPL. Fig. 4(c) shows the pair amplitude of Fig. 4(a) integrated in \mathbf{k} as a function of A_0 for distinct M . We see that M induces the spin-triplet character and A_0 enables its presence between Floquet bands [Fig. 4(a)]; the inset of Fig. 4(c) illustrates the $d_{x^2-y^2}$ -wave symmetry of the pairing. Furthermore, in Fig. 4(b,d) we show the emergent pairing with spin-triplet odd-Floquet even-frequency even-parity Cooper pairs in a p -wave UM with spin-singlet s -wave superconductivity under LPL, which are absent in the static regime. Thus, low- Ω light drives offer a broad landscape for engineering unconventional superconducting symmetries in UMs.

In conclusion, we have investigated the effect of time-periodic light drives on d -wave altermagnets and p -wave magnets, both in the normal state and when proximity-coupled to spin-singlet s -wave superconductors. We showed that the intrinsic nonrelativistic SOC in these systems leads to unconventional light-matter interactions, enabling Floquet engineering of spin-triplet states. In the high-frequency regime, linearly polarized light induces spin-triplet spin densities in d -wave altermagnets and generates tunable odd-frequency spin-triplet Cooper pairs with d - and s -wave parities. These spin-triplet

states exhibit spectroscopic signatures that can be used to probe the symmetry and strength of the altermagnetism and the type of emergent pairing. At lower drive frequencies, Floquet band mixing gives rise to additional spin-triplet pairing channels that are absent in equilibrium in d - and p -wave unconventional magnets. Our results unveil the potential of unconventional magnetism under light for Floquet engineering spin-triplet states.

P.-H. Fu acknowledges support from W. Xu. S. M. acknowledges financial support from the Göran Gustafsson Foundation (Grant No. 2216) and the Carl Trygger's Foundation (Grant No. 22: 2093). J.-F. Liu is supported by the National Natural Science Foundation of China (Grant No. 12174077). Y. T. acknowledges financial support from JSPS with Grants-in-Aid for Scientific research (KAKENHI Grants No. 23K17668 and 24K00583). J. C. acknowledges financial support from the Carl Trygger's Foundation (Grant No. 22: 2093), the Sweden-Japan Foundation (Grant No. BA24-0003), the Göran Gustafsson Foundation (Grant No. 2216), and the Swedish Research Council (Vetenskapsrådet Grant No. 2021-04121).

* phy.phfu@gmail.com

† jorge.cayao@physics.uu.se

- [1] J. Cayssol, B. Dóra, F. Simon, and R. Moessner, Floquet topological insulators, *physica status solidi (RRL)*–Rapid Research Letters **7**, 101 (2013).
- [2] M. Bukov, L. D'Alessio, and A. Polkovnikov, Universal high-frequency behavior of periodically driven systems: from dynamical stabilization to Floquet engineering, *Advances in Physics* **64**, 139 (2015).
- [3] T. Oka and S. Kitamura, Floquet engineering of quantum materials, *Annu. Rev. Condens. Matter Phys.* **10**, 387 (2019).
- [4] U. D. Giovannini and H. Hübener, Floquet analysis of excitations in materials, *J. Phys. Mater.* **3**, 012001 (2019).
- [5] M. S. Rudner and N. H. Lindner, Band structure engineering and non-equilibrium dynamics in Floquet topological insulators, *Nat. Rev. Phys.* **2**, 229 (2020).
- [6] S. Francesconi, F. Baboux, A. Raymond, N. Fabre, G. Boucher, A. Lemaitre, P. Milman, M. I. Amanti, and S. Ducci, Engineering two-photon wavefunction and exchange statistics in a semiconductor chip, *Optica* **7**, 316 (2020).
- [7] G. Floquet, Sur les équations différentielles linéaires à coefficients périodiques, *Annales scientifiques de l'École Normale Supérieure* **12**, 47 (1883).
- [8] J. H. Shirley, Solution of the schrödinger equation with a hamiltonian periodic in time, *Phys. Rev.* **138**, B979 (1965).
- [9] H. Sambe, Steady states and quasienergies of a quantum-mechanical system in an oscillating field, *Phys. Rev. A* **7**, 2203 (1973).
- [10] T. Oka and H. Aoki, Photovoltaic hall effect in graphene, *Phys. Rev. B* **79**, 081406 (2009).
- [11] T. Kitagawa, E. Berg, M. Rudner, and E. Demler, Topo-

- logical characterization of periodically driven quantum systems, *Phys. Rev. B* **82**, 235114 (2010).
- [12] N. H. Lindner, G. Refael, and V. Galitski, Floquet topological insulator in semiconductor quantum wells, *Nature Physics* **7**, 490 (2011).
- [13] J. Klinovaja, P. Stano, and D. Loss, Topological Floquet phases in driven coupled Rashba nanowires, *Phys. Rev. Lett.* **116**, 176401 (2016).
- [14] F. H. M. Faisal and J. Z. Kamiński, Floquet-bloch theory of high-harmonic generation in periodic structures, *Phys. Rev. A* **56**, 748 (1997).
- [15] T. Kitagawa, T. Oka, A. Brataas, L. Fu, and E. Demler, Transport properties of nonequilibrium systems under the application of light: Photoinduced quantum hall insulators without Landau levels, *Phys. Rev. B* **84**, 235108 (2011).
- [16] M. C. Rechtsman, J. M. Zeuner, Y. Plotnik, Y. Lumer, D. Podolsky, F. Dreisow, S. Nolte, M. Segev, and A. Szameit, Photonic Floquet topological insulators, *Nature* **496**, 196 (2013).
- [17] B. M. Fregoso, Y. H. Wang, N. Gedik, and V. Galitski, Driven electronic states at the surface of a topological insulator, *Phys. Rev. B* **88**, 155129 (2013).
- [18] Y. Wang, H. Steinberg, P. Jarillo-Herrero, and N. Gedik, Observation of Floquet-Bloch states on the surface of a topological insulator, *Science* **342**, 453 (2013).
- [19] J. W. McIver, B. Schulte, F.-U. Stein, T. Matsuyama, G. Jotzu, G. Meier, and A. Cavalleri, Light-induced anomalous Hall effect in graphene, *Nat. Phys.* **16**, 38 (2020).
- [20] S. Aeschlimann, S. A. Sato, R. Krause, M. Chávez-Cervantes, U. De Giovannini, H. Hübener, S. Forti, C. Coletti, K. Hanff, K. Rossnagel, *et al.*, Survival of Floquet-Bloch states in the presence of scattering, *Nano Lett.* **21**, 5028 (2021).
- [21] F. Mahmood, C.-K. Chan, Z. Alpichshev, D. Gardner, Y. Lee, P. A. Lee, and N. Gedik, Selective scattering between Floquet-Bloch and Volkov states in a topological insulator, *Nat. Phys.* **12**, 306 (2016).
- [22] V. Galitski and I. B. Spielman, Spin-orbit coupling in quantum gases, *Nature* **494**, 49 (2013).
- [23] A. Manchon, H. C. Koo, J. Nitta, S. M. Frolov, and R. A. Duine, New perspectives for Rashba spin-orbit coupling, *Nat. Mater.* **14**, 871 (2015).
- [24] L. Bai, W. Feng, S. Liu, L. Šmejkal, Y. Mokrousov, and Y. Yao, Altermagnetism: Exploring new frontiers in magnetism and spintronics, *Advanced Functional Materials* **34**, 2409327 (2024).
- [25] T. Jungwirth, R. M. Fernandes, E. Fradkin, A. H. MacDonald, J. Sinova, and L. Šmejkal, From superfluid ^3He to altermagnets, arXiv: 2411.00717 (2024).
- [26] T. Jungwirth, R. M. Fernandes, J. Sinova, and L. Šmejkal, Altermagnets and beyond: Nodal magnetically-ordered phases, arXiv: 2409.10034 (2024).
- [27] Y. Fukaya, B. Lu, K. Yada, Y. Tanaka, and J. Cayao, Superconducting phenomena in systems with unconventional magnets, arXiv: 2502.15400 (2025).
- [28] L. Šmejkal, J. Sinova, and T. Jungwirth, Emerging research landscape of altermagnetism, *Phys. Rev. X* **12**, 040501 (2022).
- [29] I. Mazin, Editorial: Altermagnetism—a new punch line of fundamental magnetism, *Phys. Rev. X* **12**, 040002 (2022).
- [30] B. Brekke, P. Sukhachov, H. G. Giil, A. Brataas, and J. Linder, Minimal models and transport properties of unconventional p -wave magnets, *Phys. Rev. Lett.* **133**, 236703 (2024).
- [31] A. B. Hellenes, T. Jungwirth, R. Jaeschke-Ubiergo, A. Chakraborty, J. Sinova, and L. Šmejkal, p -wave magnets, arXiv:2309.01607 (2024).
- [32] P. Sukhachov, H. G. Giil, B. Brekke, and J. Linder, Coexistence of p -wave magnetism and superconductivity, arXiv: 2412.14245 (2025).
- [33] M. Roig, A. Kreisel, Y. Yu, B. M. Andersen, and D. F. Agterberg, Minimal models for altermagnetism, *Phys. Rev. B* **110**, 144412 (2024).
- [34] B. Brekke, A. Brataas, and A. Sudbø, Two-dimensional altermagnets: Superconductivity in a minimal microscopic model, *Phys. Rev. B* **108**, 224421 (2023).
- [35] A. Zagoskin, *Quantum Theory of Many-Body Systems: Techniques and Applications* (Springer, 2014).
- [36] G. D. Mahan, *Many-particle physics* (Springer Science & Business Media, 2013).
- [37] P.-H. Fu, J. Wang, J.-F. Liu, and R.-Q. Wang, Josephson signatures of Weyl node creation and annihilation in irradiated Dirac semimetals, *Phys. Rev. B* **100**, 115414 (2019).
- [38] P.-H. Fu, Y. Xu, X.-L. Yu, J.-F. Liu, and J. Wu, Electrically modulated Josephson junction of light-dressed topological insulators, *Phys. Rev. B* **105**, 064503 (2022).
- [39] K. W. Lee, M. J. A. Calderon, X.-L. Yu, C. H. Lee, Y. S. Ang, and P.-H. Fu, Floquet engineering of topological phase transitions in a quantum spin Hall α - t_3 system, *Phys. Rev. B* **111**, 045406 (2025).
- [40] P.-H. Fu, Q. Lv, X.-L. Yu, J.-F. Liu, and J. Wu, The generation of switchable polarized currents in nodal ring semimetals using high-frequency periodic driving, *J. Phys.: Condens. Matter* **34**, 075401 (2022).
- [41] X.-S. Li, C. Wang, M.-X. Deng, H.-J. Duan, P.-H. Fu, R.-Q. Wang, L. Sheng, and D. Y. Xing, Photon-induced Weyl half-metal phase and spin filter effect from topological Dirac semimetals, *Phys. Rev. Lett.* **123**, 206601 (2019).
- [42] Z. Wang, L. Balembois, M. Rančić, E. Billaud, M. Le Dantec, A. Ferrier, P. Goldner, S. Bertaina, T. Chanelière, D. Estève, *et al.*, Single-electron spin resonance detection by microwave photon counting, *Nature* **619**, 276 (2023).
- [43] We note that low frequency CPL and LPL drives can also induce a spin-triplet density in both d - and p -wave UMs; here, the Floquet bands play a role.
- [44] F. S. Bergeret, A. F. Volkov, and K. B. Efetov, Odd triplet superconductivity and related phenomena in superconductor-ferromagnet structures, *Rev. Mod. Phys.* **77**, 1321 (2005).
- [45] Y. Tanaka, M. Sato, and N. Nagaosa, Symmetry and topology in superconductors—odd-frequency pairing and edge states—, *J. Phys. Soc. Jpn.* **81**, 011013 (2012).
- [46] J. Cayao, C. Triola, and A. M. Black-Schaffer, Odd-frequency superconducting pairing in one-dimensional systems, *Eur. Phys. J. Spec. Top.* **229**, 545 (2020).
- [47] J. Linder and A. V. Balatsky, Odd-frequency superconductivity, *Rev. Mod. Phys.* **91**, 045005 (2019).
- [48] C. Triola, J. Cayao, and A. M. Black-Schaffer, The role of odd-frequency pairing in multiband superconductors, *Ann. Phys.* **532**, 1900298 (2020).
- [49] Y. Tanaka, S. Tamura, and J. Cayao, Theory of Majorana zero modes in unconventional superconductors,

- Prog. Theor. Exp. Phys. **2024**, 08C105 (2024).
- [50] K. Maeda, Y. Fukaya, K. Yada, B. Lu, Y. Tanaka, and J. Cayao, Classification of pair symmetries in superconductors with unconventional magnetism, Phys. Rev. B **111**, 144508 (2025).
- [51] Y. Fukaya, K. Maeda, K. Yada, J. Cayao, Y. Tanaka, and B. Lu, Josephson effect and odd-frequency pairing in superconducting junctions with unconventional magnets, Phys. Rev. B **111**, 064502 (2025).
- [52] Q. P. Li, B. E. C. Koltenbah, and R. Joynt, Mixed s-wave and d-wave superconductivity in high- T_c systems, Phys. Rev. B **48**, 437 (1993).
- [53] C. O'Donovan and J. P. Carbotte, s- and d-wave mixing in high- t_c superconductors, Phys. Rev. B **52**, 16208 (1995).
- [54] T. Hanaguri, Y. Kohsaka, J. Davis, C. Lupien, I. Yamada, M. Azuma, M. Takano, K. Ohishi, M. Ono, and H. Takagi, Quasiparticle interference and superconducting gap in $\text{Ca}_2\text{-xNa}_x\text{CuO}_2\text{Cl}_2$, Nat. Phys. **3**, 865 (2007).
- [55] R. Sharma, S. D. Edkins, Z. Wang, A. Kostin, C. Sow, Y. Maeno, A. P. Mackenzie, J. S. Davis, and V. Madhavan, Momentum-resolved superconducting energy gaps of Sr_2RuO_4 from quasiparticle interference imaging, Proc. Natl. Acad. Sci. **117**, 5222 (2020).
- [56] M. P. Allan, A. W. Rost, A. Mackenzie, Y. Xie, J. Davis, K. Kihou, C.-H. Lee, A. Iyo, H. Eisaki, and T.-M. Chuang, Anisotropic energy gaps of iron-based superconductivity from intraband quasiparticle interference in lifeas, Science **336**, 563 (2012).
- [57] We note that the same conclusions can be obtained from the imaginary part $\text{Im}\bar{F}_t^{\text{eff}}$ demonstrating peak-dip structures and competition between $\text{Im}\bar{F}_{t,M}^{\text{eff}}$ and $\text{Im}\bar{F}_{t,\Omega}^{\text{eff}}$.
- [58] S. Kashiwaya and Y. Tanaka, Tunnelling effects on surface bound states in unconventional superconductors, Rep. Prog. Phys. **63**, 1641 (2000).
- [59] J. C. Cuevas, A. Martín-Rodero, and A. L. Yeyati, Hamiltonian approach to the transport properties of superconducting quantum point contacts, Phys. Rev. B **54**, 7366 (1996).
- [60] P. Buset, B. Lu, H. Ebisu, Y. Asano, and Y. Tanaka, All-electrical generation and control of odd-frequency s-wave cooper pairs in double quantum dots, Phys. Rev. B **93**, 201402 (2016).
- [61] E. Ahmed, S. Tamura, Y. Tanaka, and J. Cayao, Odd-frequency superconducting pairing due to multiple majorana edge modes in driven topological superconductors, Phys. Rev. B **111**, 024507 (2025).
- [62] J. Cayao, P. Buset, and Y. Tanaka, Controllable odd-frequency cooper pairs in multiferroic josephson junctions, Phys. Rev. B **109**, 205406 (2024).
- [63] J. Cayao, C. Triola, and A. M. Black-Schaffer, Floquet engineering bulk odd-frequency superconducting pairs, Phys. Rev. B **103**, 104505 (2021).
- [64] T. Kuhn, B. Sothmann, and J. Cayao, Floquet engineering higgs dynamics in time-periodic superconductors, Phys. Rev. B **109**, 134517 (2024).